Temperature Dependence of Circular Dichroism and Fluorescence Decay of Pyrene Appended to the Side Chains of Poly-L-glutamine

Osami Shoji,† Daisuke Nakajima, and Masahiro Ohkawa

Graduate School of Science and Technology, Chiba University, Yayoi-cho 1-33, Inage-ku, Chiba 263-8522, Japan

Yoshiki Fujiwara, Masahiko Annaka, Masako Yoshikuni, and Takayuki Nakahira*

Department of Materials Technology, Faculty of Engineering, Chiba University, Yayoi-cho 1-33, Inage-ku, Chiba 263-8522, Japan

Received December 5, 2002; Revised Manuscript Received March 24, 2003

ABSTRACT: The temperature dependence of side-chain chromophore orientation and excimer formation in diastereomeric poly[N^5-(*R* and *S*)-1-(1-pyrenyl)ethyl-L-glutamines] (**1** and **2**) was examined in DMAc using circular dichroic (CD) and fluorescence spectroscopy. In comparison with **1**, **2** afforded CD spectra suggesting a better controlled pyrene chromophore orientation. It, however, gave a stronger excimer fluorescence. Assuming that a major portion of excimers are formed in the portions of the polymer where the side chains are disordered, the ratios of ordered side chains to disordered side chains, i.e., the equilibrium constants between the two side-chain structures, were evaluated from fluorescence decay analysis. The equilibrium constants were found to be consistently smaller for **2** than for **1** in the temperature range examined. The stronger excimer emission observed with **2** is thus suggested due to the larger content of disordered side chains in **2** despite the better controlled chromophore orientation in its ordered side chains. This is consistent with the lower activation energy of excimer formation estimated for **2**. The molar ellipticities of the ordered and disordered side chains were evaluated from the observed CD and the equilibrium constants. The possible ordered side-chain structures of **1** and **2** were explored by molecular mechanics calculations as well as theoretical CD calculations based on the low-energy conformations obtained thereby.

Introduction

The crystal structure of the photosystem in photosynthetic bacteria has been revealed by X-ray crystal analysis, showing that the arrangement of the light-harvesting antenna pigments is highly controlled by polypeptide frameworks so as to bring rapid and efficient excitation energy transport to the photochemical reaction center.[1−3] Polypeptides may thus be considered as promising molecular frameworks to arrange photofunctional chromophores in artificial photosynthesis and other photoelectronic processes.[4−8] If the orientation of the chromophores in the side chains of a helical polypeptide is highly controlled, we would have "molecular wires" capable of efficiently transporting excitation energy along the polymer backbone.[9−15]

In the previous studies, we prepared poly(L-glutamines) having naphthalene and pyrene chromophores in the side chains, i.e., poly[N^5-(*R* and *S*)-1-(1-naphthyl)ethyl-L-glutamines],[7,16] poly[N^5-1-naphthylmethyl-L-glutamine],[16] and poly(N^5-1-pyrenylmethyl-L-glutamine),[17] and examined their side-chain chromophore orientation along the helical main chain by CD and fluorescence spectroscopy. Examining the CD signals in relation to the side-chain chromophore structure, we concluded that the chirality in the side chain, i.e., introduction of methyl groups near the chromophores, and the bulkiness of the chromophore itself contribute greatly to the side-chain chromophore orientation and suppression of excimer formation in poly(L-glutamines). More recently, we examined poly[N^5-(*R* and *S*)-1-(1-pyrenyl)ethyl-L-glutamines] (**1** and **2**) and further confirmed the importance of the specific steric interactions among the bulky chiral side chains in controlling side-chain orientation:[18] **2** was found to give strong CD signals, indicative of highly controlled chromophore orientation, whose intensities increase as the solvent is changed from DMAc to THF. **1**, on the other hand, changed the signs of relatively weak CD signals upon the solvent change, suggesting that chromophore orientation of **1** is not as firmly controlled as that of **2**. **2**, however, showed stronger excimer emission than **1** in both solvents. (Intense excimer emission is attributed either to a large

Scheme 1. Polymers and Low-Molecular-Weight Model Compounds

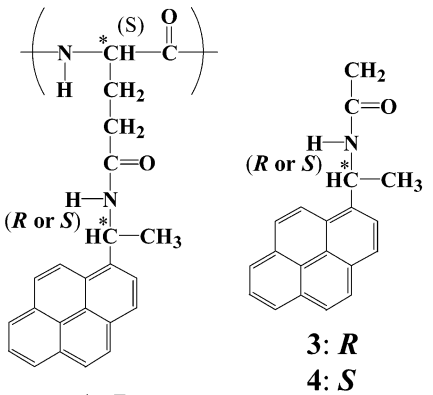

1: ***R***
2: ***S***

3: ***R***
4: ***S***

* To whom correspondence should be addressed.

† Taken in part from the Doctoral Thesis of O.S. submitted to Graduate School of Science and Technology, Chiba University.

10.1021/ma025922w CCC: $25.00
Published on Web 05/14/2003

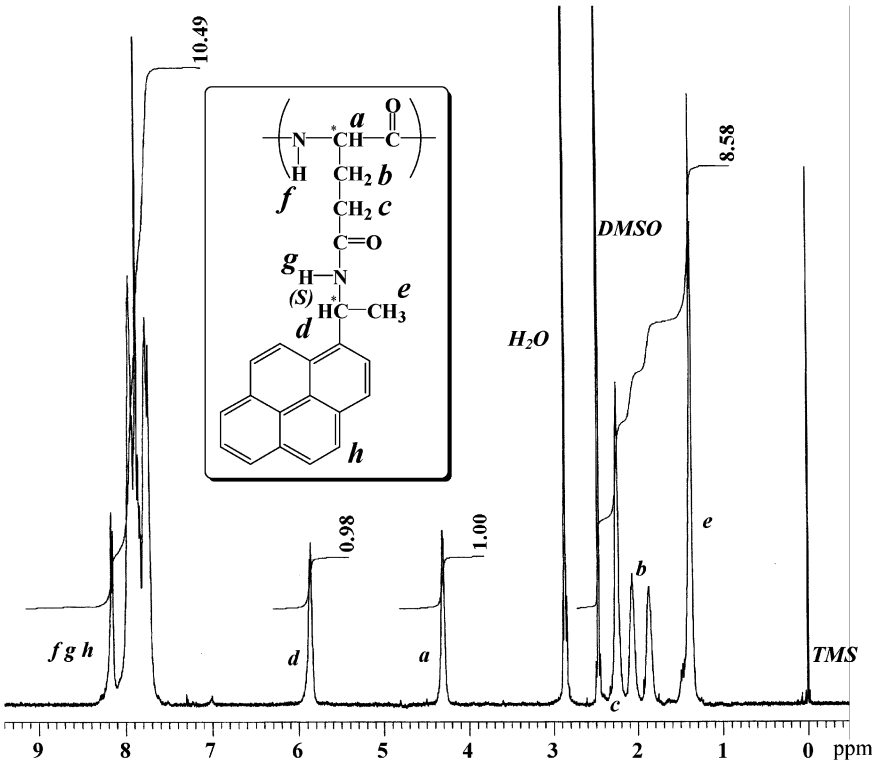

Figure 1. 500 MHz ^{1}H NMR spectrum of **2** in DMSO-d_6 at 120 °C.

number of excimer forming sites where two pyrene chromophores are situated in close proximity to each other with a suitable geometry for excimer formation or to efficient excitation energy transport among pyrene chromophores to those sites.)

In the present study, we examined the CD and fluorescence spectra of **1** and **2** in DMAc as a function of temperature so as to gain further insight into the control of chromophore orientation along the helical main chain. We also carried out molecular mechanics calculations to examine the side-chain chromophore orientation in the ordered side chains of **1** and **2** (Scheme 1). We are particularly interested in how the hydrogen-bonding interactions among the side-chain and main-chain amide groups contribute to control of side-chain chromophore orientation.

Experimental Section

Materials. Racemic 1-(1-pyrenyl)ethylamine was synthesized from 1-acetylpyrene, formic acid, and formamide using the Leuckart reaction.[19] Optical resolution was accomplished by repeated crystallization of salts formed with *d*- or *l*-tartaric acid.[20] The optical purity was checked by ^{1}H NMR in the presence of 2 equiv of (*R*)-1,1′-bi-2-naphthol in $CDCl_3$.[21] The absolute configuration of (*R*)-1-(1-pyrenyl)ethylamine was established by X-ray crystal structural analysis of its ammonium salt single crystal formed with (1*S*)-10-camphorsulfonic acid. The analysis was carried out by the direct method,[22] expanded by Fourier techniques[23] and refined by the full-matrix least-squares method, where the final R and R_w were 0.058 and 0.057 for 2055 reflections, indicating a space group $P2_1$ with $a = 9.980(9)$ Å, $b = 7.735(2)$ Å, $c = 16.16(1)$ Å, $\beta = 91.41(5)°$, $V = 1246(1)$ Å^3, $Z = 2$, $D_{calc} = 1.272$ g/cm^3, and μ(Cu Kα) = 1.64 cm^{-1}. The optical rotation ($[\alpha]^{25}_D$) of (*R*)-1-(1-pyrenyl)ethylamine and that of (*S*)-1-(1-pyrenyl)ethylamine were +82.1 ($c = 0.84$ g dL^{-1}) and −81.8° ($c = 0.90$ g dL^{-1}) in THF, respectively.

1 and **2** were prepared from poly(L-glutamic acid) (DP 385, Aldrich Co.) and (*R*)- and (*S*)-1-(1-pyrenyl)ethylamines with an amine to carboxylic acid molar ratio of 2 using *N*,*N*-dicyclohexylcarbodiimide and 1-hydroxybenzotriazole as condensing agents as previously described.[7,17] Full derivatization of the side-chain carboxyl groups was confirmed by 500 MHz ^{1}H NMR in DMSO-d_6 at 120 °C as shown in Figure 1. The DP 70 samples were similarly prepared for IR measurements. The monomeric model compounds, *N*-(*R* and *S*)-1-(1-pyrenyl)-ethylacetamides (**3** and **4**), were prepared from the corresponding amines and acetyl chloride in THF.

Measurements. ^{1}H NMR spectra were measured using a JEOL LA-500 MHz spectrometer. X-ray crystallographic analysis was carried out on a Rigaku RAXIS-II diffractometer with graphite monochromated Mo Kα radiation. Optical rotations were recorded on a JASCO DIP-370 polarimeter. UV and steady-state fluorescence spectra were recorded on a Hitachi U-3210 spectrophotometer and on a Hitachi F-4010 fluorescence spectrophotometer, respectively. CD spectra were measured on a JASCO J-820 circular dichrograph.

IR spectra were recorded on a JASCO JIR-7000 FT-IR spectrophotometer. Curve fitting was performed with the peak fitting module of Origin software (Microcal Software, Inc., New York). The Voigt function, a sum of Gaussian and Lorentzian band shapes, was used as a fitting function.

Fluorescence decays were measured by time-correlated single photon counting using an IBH 5000U spectrophotometer. The decays of emission, monitored at 377 nm, were fitted with double-exponential functions, i.e., $I_M(t) = A_1 \exp(-t/\tau_{M1}) + A_2 \exp(-t/\tau_{M2})$. In all cases, the dynamic range used in fitting was set to 50. The decays at 40 °C and their fitting to double-exponential functions are shown in Figure 2. The decay parameters at various temperatures are given in Table 1. The fits, except those of **2** at 20 and 50 °C, are regarded reasonable as judged from the χ^2 values.

Molecular Mechanics Calculations. Molecular mechanics calculations were carried out by employing the same procedure as described for poly(N^5-1-pyrenylmethyl-L-glutamine).[17] Initially, the low-energy conformations for the respective polymer were explored using the PEPCON program,[24] in which the dihedral angles of the main chain were fixed at those of the right-handed α-helix ($\phi = -62.5°$, $\psi = -42.3°$, and $\omega = 180°$)[25] and that of χ^4 at 180° while χ^1, χ^2, χ^3, χ^5, and χ^6 (Scheme 2) were varied with 30° intervals assuming all the monomer units have a common conformation. The first 100 low-energy

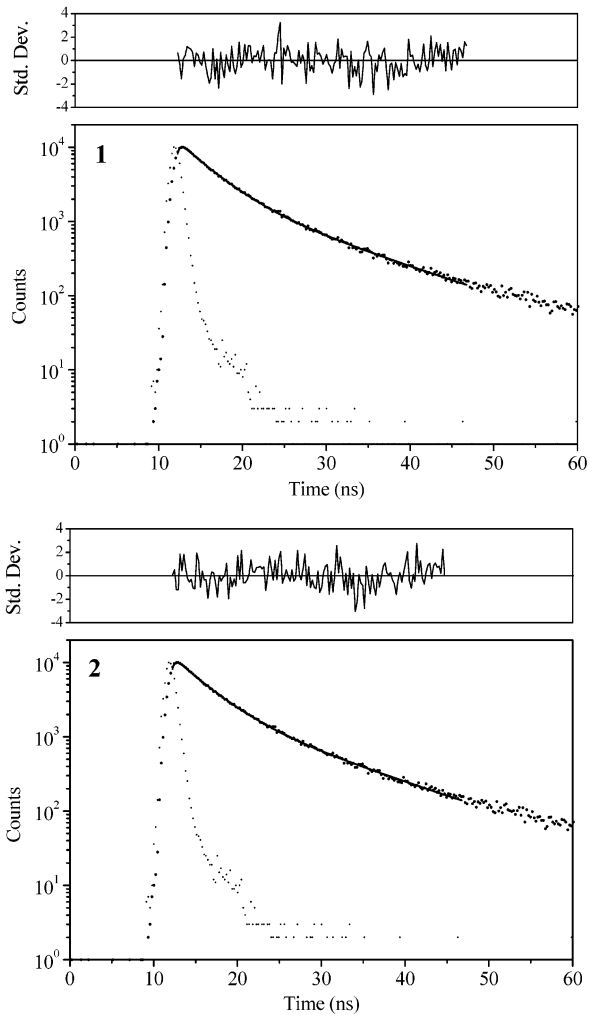

Figure 2. Decays of monomer emission from **1** and **2** monitored at 377 nm in DMAc at 40 °C. $\lambda_{ex} = 282$ nm; [Py] = 2.0×10^{-5} M. The decays are fitted as follows. **1**: $I_M(t) = 0.156 \exp(-t/3.56\text{ ns}) + 0.0409 \exp(-t/11.7\text{ ns})$ $\chi^2 = 1.134$. **2**: $I_M(t) = 0.161 \exp(-t/3.29\text{ ns}) + 0.0353 \exp(-t/11.9\text{ ns})$ $\chi^2 = 1.159$.

Table 1. Fluorescence Decay Parameters of 1 and 2

sample	temp (°C)	A_1	τ_{M1}(ns)	A_2	τ_{M2}(ns)	χ^2	A_2/A_1
1	20	0.114	5.7	0.064	16.0	1.358	0.56
	30	0.135	4.5	0.052	13.4	1.396	0.39
	40	0.156	3.6	0.041	11.7	1.134	0.26
	50	0.174	2.9	0.035	10.6	1.265	0.20
	60	0.189	2.4	0.032	9.9	1.162	0.17
2	20	0.134	5.1	0.049	15.9	1.631	0.37
	30	0.140	4.0	0.045	12.9	1.130	0.32
	40	0.161	3.3	0.035	11.9	1.159	0.22
	50	0.178	2.5	0.035	10.4	1.481	0.20
	60	0.180	2.2	0.029	10.5	1.316	0.16

conformations thus obtained were optimized with respect to χ^1, χ^2, χ^3, χ^5, and χ^6. They afforded 25 low-energy conformations for **1** and 21 of those for **2**. When the 40-mers of these conformations were subjected to full optimization with respect to all the structural parameters using the CAChe MM2 program,[26] they converged to six and seven low-energy conformations for **1** and for **2**, respectively (Tables 2 and 3). When a periodicity emerged among the conformations of the side chains, the monomer units which compose the periodicity were treated as a repeating unit, polymerized, and optimized further. The secondary hydrogen bonds in three-center hydrogen bonding in α-helical main chain, i.e., the $i/(i + 3)$ main-chain hydrogen bonds formed between the ith and $(i + 3)$th monomer units,[27] as evaluated by the MM2 calculations, have

Scheme 2. Definition of Dihedral Angles

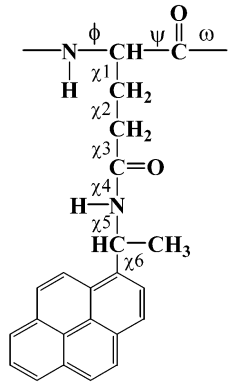

an average H···O distance of 2.3 Å and average N−H···O and H···O=C angles of 115 and 95°, as compared with the corresponding values of 2.1 Å, 145°, and 145° for the primary $i/(i + 4)$ main-chain hydrogen bonds. In the case of the secondary hydrogen bonds in "multicenter" hydrogen bonding involving side-chain amide groups, the corresponding values are 2.6 ± 0.3 Å, 120 ± 30°, and 120 ± 30°.

Theoretical CD Calculations. Theoretical CD calculations[28] were carried out as described previously.[17] In the present study, the ^1L_a and ^1B_b absorptions bands were deconvoluted into vibronic peaks. Each vibronic peak was regarded as a separate transition and fitted with a Gaussian function. The magnitude of the transition moment for each vibronic peak was determined as described in the literature,[28] its direction being assumed to be common among all the vibronic peaks in the same absorption band.[29−31] The mutual orientation of the transition moments of the neighboring pyrene groups and their positions were determined from the geometries obtained by the molecular mechanics calculations. Only the interactions between the like transitions were taken into consideration and the overall CD was estimated as a sum of exciton interactions between various pairs of pyrene groups.

Results and Discussion

Temperature Dependence of CD Spectra. In Figure 3 are shown the CD spectra of **1** and **2** in DMAc as a function of temperature. As previously noted, the CD signals of **1** and **2** in the pyrene absorption bands, except that of **1** in the ^1B_b band, are much stronger than those of corresponding monomeric model compounds and show splitting indicative of positive exciton coupling among the side-chain pyrene chromophores. The CD signal of **1** in the ^1B_b band is virtually identical to that of the monomeric model compound, apparently reflecting only the local chirality in the individual side chain. The weaker CD signals in the ^1L_a band as well as the absence of exciton coupling in the ^1B_b band suggests that the pyrene chromophore orientation of **1** is not as well controlled as that of **2**.

The CD spectra of **1** and **2** showed monotonic increase in intensity upon cooling from 80 to 0 °C. (Contrary to our expectation, **1** did not change signs of CD signals as observed upon change of solvent from DMAc to THF.[18]) These changes were reversible. Since we can expect that the main chain takes helical conformation under the present conditions,[7] the increased CD intensities at lower temperatures may be attributed to the increased population of the ordered side chains. Assuming that equilibrium is established between the disordered and ordered side chains, we have

$$K = [\text{ordered side chains}]/[\text{disordered side chains}] = \exp(-\Delta H°/RT + \Delta S°/R) \quad (1)$$

Table 2. Optimized Conformations of 1 by CAChe

conformation	conformational energy (kcal/monomer unit mol)	dihedral angles (deg)								
		φ	ψ	ω	χ^1	χ^2	χ^3	χ^4	χ^5	χ^6
R1	−49.82	−68.1[a] ± 6.6[b]	−36.4 ± 7.4	179.1 ± 5.6	189.6 ± 3.7	276.8 ± 2.1	177.4 ± 3.7	177.3 ± 6.2	116.9 ± 9.9	6.9 ± 8.3
R2	−47.85	−63.8 ± 13.3	−39.6 ± 10.6	179.2 ± 6.8	288.5 ± 24.5	163.0 ± 20.7	58.6 ± 5.5	200.0 ± 8.6	89.8 ± 16.1	21.8 ± 8.2
R3	−47.62	−70.1 ± 12.6	−37.2 ± 17.6	177.5 ± 4.5	182.6 ± 13.6	58.5 ± 15.3	63.0 ± 12.6	190.4 ± 9.7	94.8 ± 51.0	23.2 ± 23.3
R4	−47.27	−60.0 ± 1.3	−40.0 ± 1.6	177.5 ± 1.2	178.3 ± 0.8	281.2 ± 0.5	292.5 ± 1.0	161.9 ± 3.5	55.7 ± 2.4	30.0 ± 1.4
R5	−46.95	−61.2 ± 22.6	−42.3 ± 17.2	178.2 ± 4.2	269.6 ± 9.3	51.1 ± 6.9	180.8 ± 20.2	179.6 ± 5.6	104.7 ± 17.3	10.4 ± 8.0
R6	−46.26	−63.4 ± 11.6	−39.6 ± 12.4	180.2 ± 5.0	294.0 ± 30.4	297.5 ±9.8	143.9 ± 47.7	181.9 ± 21.4	101.0 ± 35.5	50.7 ± 48.5

[a] The average of 10 monomer units in the middle of the 40-mer. [b] Maximum deviation from the average.

Table 3. Optimized Conformations of 2 by CAChe

conformation	conformational energy (kcal/monomer unit mol)	dihedral angles (deg)								
		φ	ψ	ω	χ^1	χ^2	χ^3	χ^4	χ^5	χ^6
S1	−48.64	−70.2[a] ± 9.5[b]	−34.6 ± 12.2	178.4 ± 1.9	201.0 ± 11.7	65.9 ± 3.0	179.9 ± 9.3	174.3 ± 9.8	263.7 ± 10.7	320.2 ± 13.6
S2	−47.72	−71.7 ± 16.7	−35.5 ± 13.9	176.8 ± 2.1	154.4 ± 6.5	284.8 ± 3.9	167.8 ± 4.4	179.1 ± 3.3	292.9 ± 2.8	322.2 ± 8.3
S3	−47.12	−61.9 ± 7.2	−41.4 ± 7.5	180.1 ± 1.4	285.0 ± 2.9	184.2 ± 1.1	184.5 ± 4.0	173.9 ± 1.4	282.2 ± 2.6	337.6 ± 4.1
S4	−46.90	−69.8 ± 10.5	−38.4 ± 17.1	181.5 ± 5.3	295.7 ± 3.8	169.1 ± 7.3	299.1 ± 6.2	176.6 ± 6.9	233.8 ± 16.2	355.5 ± 5.1
S5	−46.62	−72.1 ± 20.0	−36.6 ± 16.0	177.0 ± 6.1	173.4 ± 5.1	252.4 ± 18.3	232.6 ± 22.3	167.7 ± 7.6	273.0 ± 12.5	328.4 ± 6.0
S6	−46.35	−65.8 ± 12.6	−39.5 ± 16.2	181.0 ± 4.9	192.5 ± 16.9	188.4 ± 11.6	288.4 ± 8.8	175.2 ± 7.6	265.8 ± 14.1	327.6 ± 12.3
S7	−46.26	−74.8± 17.9	−32.9 ± 13.3	175.8 ± 3.6	164.5 ± 9.1	280.5 ± 4.1	182.4 ± 6.1	181.6 ± 3.8	304.5 ± 4.4	332.3 ± 3.0

[a] The average of 10 monomer units in the middle of the 40-mer. [b] Maximum deviation from the average.

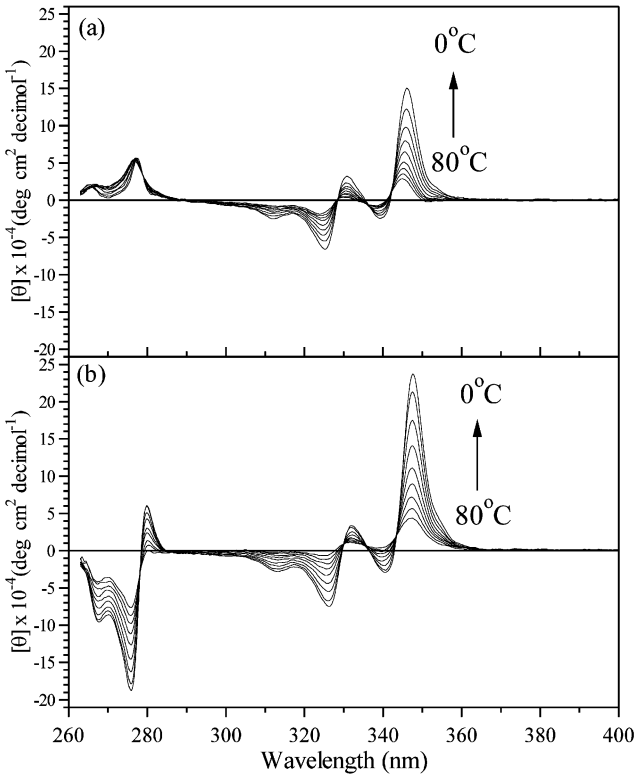

Figure 3. Temperature dependence of CD spectra of (a) **1** and (b) **2** in DMAc. [Py] = 1.0×10^{-4} M; cell length 2 mm. Temperatures are 80, 70, 60, 50, 40, 30, 20, 10, and 0 °C. The CD intensities are expressed in terms of pyrene concentration.

where $\Delta H°$ and $\Delta S°$ are the enthalpy and entropy differences between the disordered and ordered side chains. The molar ellipticity at a particular wavelength (347 nm) at each temperature $[\theta]_{observed}$ will then be given as

$$[\theta]_{observed} = x[\theta]_{ordered} + (1 - x)[\theta]_{disordered} \qquad (2)$$

where x is the fraction of the ordered side chains, i.e., $x = K/(1 + K)$, and $[\theta]_{ordered}$ and $[\theta]_{disordered}$ are the molar ellipticities for the ordered side chains and for the disordered side chains, respectively. Equilibrium constant K at each temperature is estimated from fluorescence decay measured in DMAc at each temperature, i.e., from 20 to 60 °C. The decay of 377 nm pyrene emission can be fitted with a double exponential decay function, suggesting that each polymer has two kinetically distinct excited pyrene species at each temperature.[10] (As seen later, dissociation of excimers to excited and ground-state pyrene monomers apparently does not occur in the temperature range examined. Excimer emission decays with a common lifetime of 32 ns with a rise for **2** faster than for **1**.) The excited pyrene chromophores in disordered side chains would have a shorter lifetime as they would easily form excimers. We thus assign the shorter lifetime component τ_{M1} to the pyrene chromophores in the disordered side chains and the longer lifetime component τ_{M2} to those in the ordered side chains. K at each temperature is thus estimated as the ratio of the preexponential factors, i.e., A_2/A_1 (Table 1). **2** is shown to have a smaller K and thus a smaller fraction of ordered side chains than **1** in the temperature range examined. The plots of ln K against $1/T$ gave straight lines as shown in Figure 4, allowing one to evaluate $\Delta H°$ and $\Delta S°$ from the slopes and intercepts. $\Delta H°$ and $\Delta S°$ are −5.9 kcal/mol residue and −21 cal/K/mol residue for **1** and −4.4 kcal/mol residue and −17 cal/K/mol residue for **2**. $[\theta]_{ordered}$ and $[\theta]_{disordered}$ for **1**, estimated by plotting $[\theta]_{observed}$ against x (Figure 5), are 2.6×10^5 and 9.5×10^3 deg cm^2 dmol^{-1} (346 nm) while those for **2** are 6.4×10^5 and -1.5×10^4 deg cm^2 dmol^{-1} (348 nm). The $[\theta]_{disordered}$ values are somewhat intriguing at first glance as they differ from the $[\theta]$ values of the corresponding monomeric model compounds, i.e., -1.3×10^4 and $+1.3 \times 10^4$ deg cm^2 dmol^{-1} (346 nm) for **3** and **4**, respectively.[18] We presume that the chromophores in the disordered side chains are still confined in the chiral environment provided by the main chain and the neighboring side chains. Plots of $[\theta]_{observed}$ at different wavelengths against x similarly afforded straight lines, giving $[\theta]_{ordered}$ and $[\theta]_{disordered}$ values of, for example, -1.2×10^5 and -8.9×10^3 deg cm^2 dmol^{-1} (325 nm) for **1** and -2.3×10^5 and $+1.5 \times 10^4$ deg cm^2 dmol^{-1} (326 nm) for **2**.

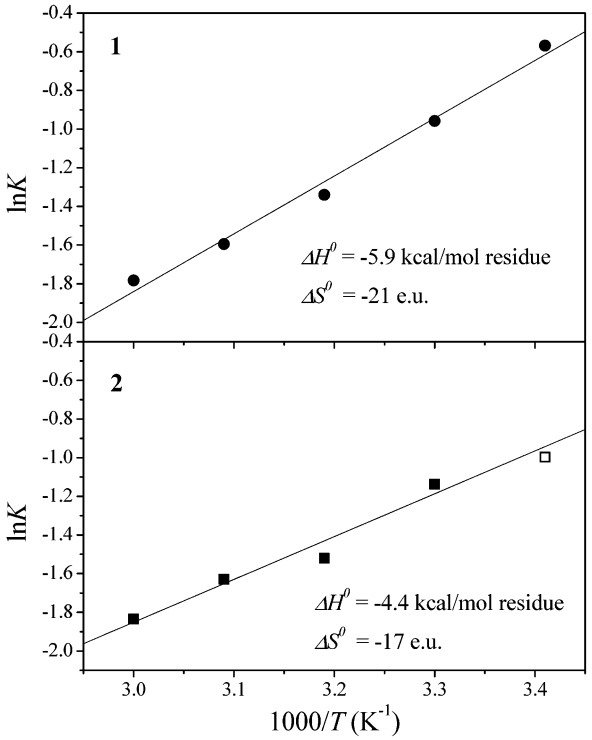

Figure 4. Plots of equilibrium constant K of **1** (●) and **2** (■) against the reciprocal of temperature. In fitting to a straight line, the datum of **2** at 20 °C (□) is omitted due to uncertainty in K.

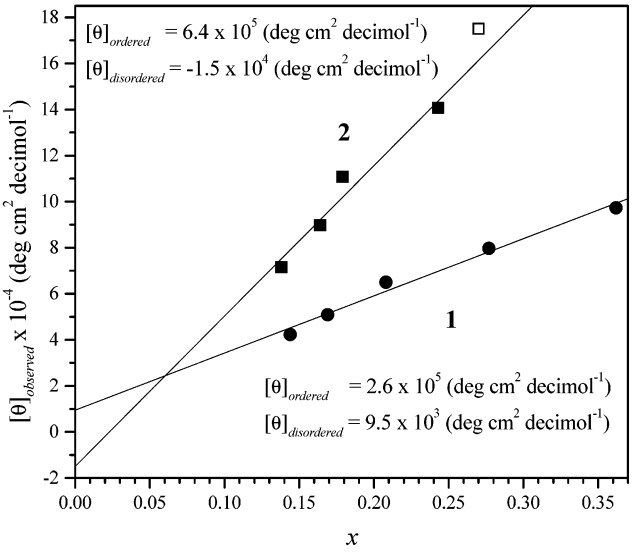

Figure 5. Plots of $[\theta]_{observed}$ against x for **1** (●) at 346 nm and **2** (■) at 348 nm. In fitting to a straight line, the datum of **2** at 20 °C (□) is omitted as in Figure 4.

Temperature Dependence of Excimer Emission. As previously reported,[18] **1** and **2** show relatively strong excimer emission around 470 nm. Relative to monomer emission I_M, excimer emission I_D is stronger with **2** than with **1**. The temperature dependence of fluorescence spectra is shown in Figure 6. If we assume that simple Birks' kinetics[32] applies to the present case, the ratio of excimer emission to monomer emission under photostationary conditions is given by

$$\frac{\Phi_D}{\Phi_M} = \frac{k_{FD}k_{DM}}{k_{FM}(k_D + k_{MD})} \qquad (3)$$

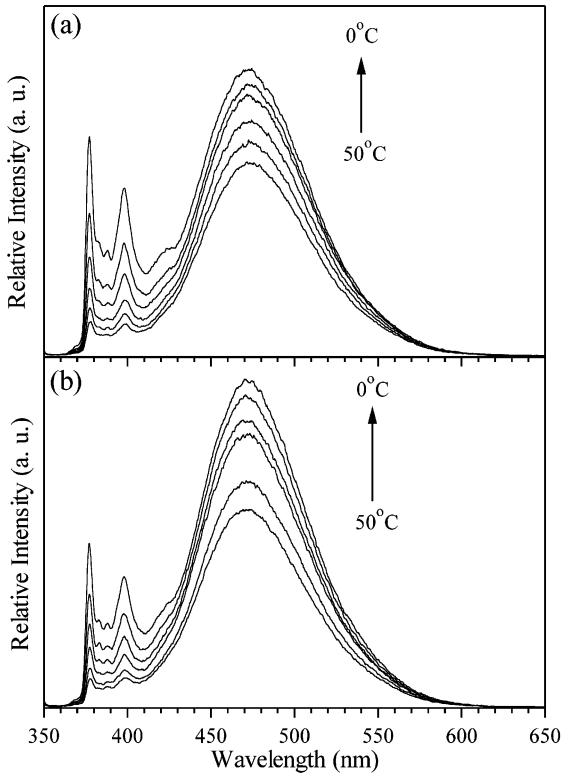

Figure 6. Temperature dependence of fluorescence spectra of (a) **1** and (b) **2** in DMAc. λ_{ex} = 345 nm; [Py] = 5.0 × 10^{-6} M. Temperatures are 50, 40, 30, 20, 10, and 0 °C.

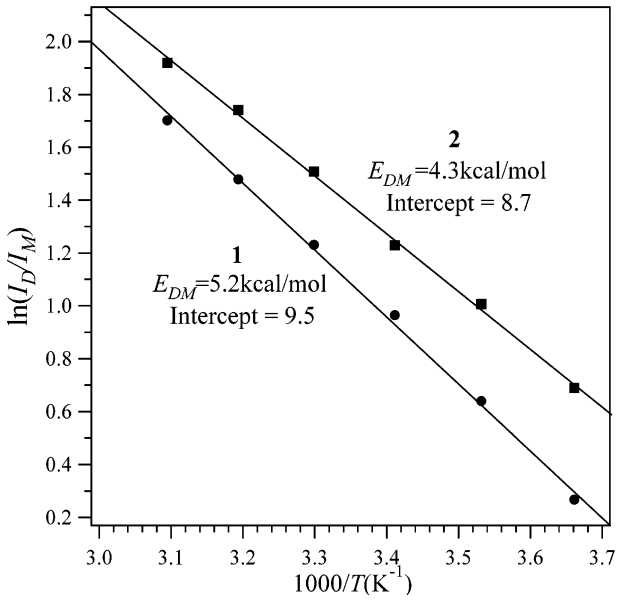

Figure 7. Plots of the natural logarithm of excimer to monomer emission intensity ratios (I_D/I_M) of **1** (●) and **2** (■) against the reciprocal of temperature. I_D and I_M were measured at 377 nm and at 470 nm, respectively.

where k_{FM} and k_{FD} are the radiative rate constants of excited monomer and excimer, k_{DM} and k_{MD} are the rate constants of excimer formation and excimer dissociation, and k_D is the sum of radiative and nonradiative decay rate constants of excimer, i.e., $k_D = k_{FD} + k_{ID}$.

The plots of $\ln(I_D/I_M)$ against the reciprocal of temperature are shown in Figure 7. The linear plots with negative slopes indicate the "low-temperature region" where excimer dissociation is negligible, i.e., $k_D \gg k_{MD}$.[32] In the "low-temperature region", we can also assume

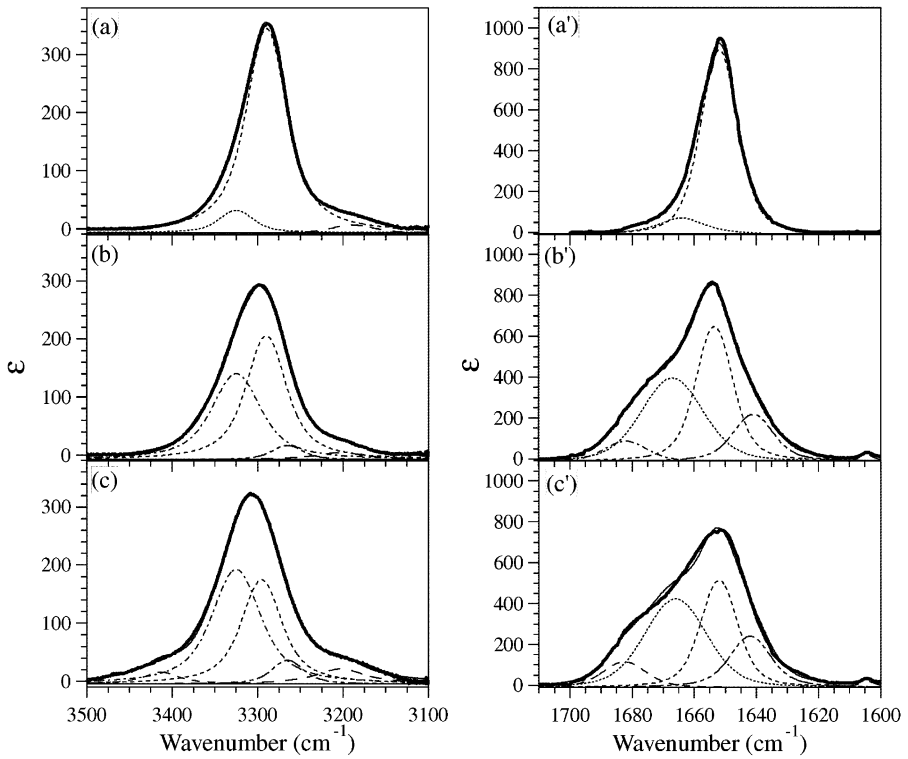

Figure 8. Amide carbonyl and amide N−H absorptions of poly(γ-benzyl-L-glutamate) **(**a, a′), **1** (b, b′), and **2** (c, c′) in THF. Curve fitting using Voigt functions are also shown. Concentrations in terms of monomer unit: $1.5-3.0 \times 10^{-3}$ M. Spacer length: 1 mm.

$k_{ID} = (k^0_{ID} + k_{ID}' \exp(-E_{ID}/RT)) \approx k^0_{ID}$, where k^0_{ID} is the temperature-independent portion of the thermal decay rate constant of excimer. (3) thus reduces to

$$\frac{\Phi_D}{\Phi_M} = \frac{k_{FD}k_{DM}}{k_{FM}(k_{FD} + k^0_{ID})} \quad (4)$$

Since all the rate constants except k_{DM} are assumed to be independent of temperature, $\ln(I_D/I_M)$ is given as

$$\ln\left(\frac{I_D}{I_M}\right) = \ln(k^0_{DM}) - \frac{E_{DM}}{RT} + \ln\left(\frac{k_{FD}}{k_{FM}(k_{FD} + k^0_{ID})}\right) + \ln C \quad (5)$$

where k^0_{DM} and E_{DM} are the preexponential factor and the activation energy of excimer formation, respectively, and C is a correction factor for the emission intensity ratios as they are evaluated from emission peak intensities, not from actual fluorescence quantum yields. The activation energies of excimer formation calculated from the slopes are 5.2 kcal/mol residue for **1** and 4.3 kcal/mol residue for **2**, suggesting that pyrene chromophores in **2** require a smaller activation energy to form excimers. (The activation energy of a low-molecular compound, i.e., meso-2,4-di(2-pyrenyl)pentane, is reported to be 3.8 kcal/mol in isooctane.[33]) The extrapolated intercept, on the other hand, is more positive for **1** than for **2**. The intercept should reflect the preexponential factor k^0_{DM} as the last two terms in (5) should be common in the two polymers, suggesting a less negative entropy of activation for excimer formation in **1**.

In evaluating the activation energy of excimer formation, we did not take into account the presence of the disordered and ordered side chains. We believe that the larger overall activation energy estimated for **1** should reflect, at least in part, the increased population of the ordered side chains as the ordered side chains are expected to require a higher activation energy of excimer formation than the disordered ones.

Ordered Side-Chain Structures as Explored by Molecular Mechanics and Theoretical CD Calculations. Molecular mechanics calculations afforded low-energy conformations **R1**−**R6** for **1** and **S1**−**S7** for **2** (Tables 2 and 3). Those conformations that have large deviations (>±10°) in dihedral angles among the monomer units have periodicity in dihedral angle distribution. Among these, **R3**, **R4**, **R5**, **S2**, and **S4** form hydrogen bonds either among the side-chain amide groups or between the side-chain and main-chain amide groups. Since the IR spectra of **1** and **2** in THF (Figure 8) show considerable decrease of 3290 and 1650 cm^{-1} absorptions characteristic of α-helical main chain as compared with that of a typical α-helical polypeptide, i.e., poly(γ-benzyl-L-glutamate), some of the side-chain amide groups are likely to undergo intramolecular hydrogen bonding, thereby deforming the α-helical main chain. We therefore selected the above five as candidates for the structures of ordered side chains.

R3 has a conformational periodicity composed of six monomer units and in each period forms one hydrogen bond ($r_{H\cdots O} = 2.2 \pm 0.2$ Å, ∠N−H···O ≈ ∠H···O=C = 149 ± 2°) between the side-chain amide carbonyl and side-chain amide NH groups, e.g., that between the 20th and 24th monomer units depicted in the top view of **R3** in Figure 9. (The monomer units are numbered from the N-terminal.) By doing so, however, it breaks consecutive two secondary $i/(i + 3)$ hydrogen bonds in the main chain,[27] thereby deforming the main-chain α-helix.

R5 also has a slight periodicity in dihedral distribution, again composed of six monomer units, and shows continuous formation of hydrogen bonds between the

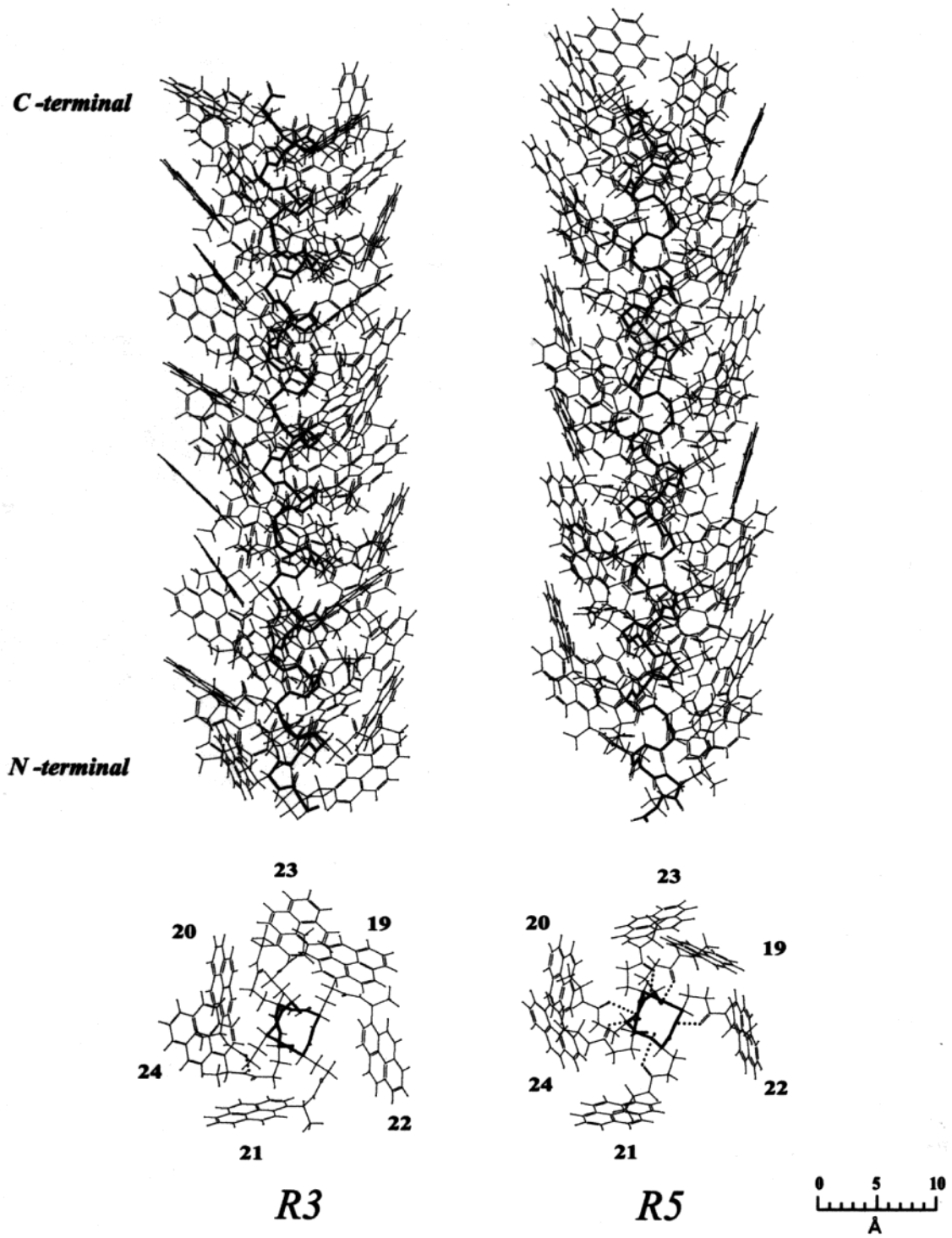

Figure 9. Side views and top views (six monomer units in the middle of polymer) of **R3** and **R5**. Dotted lines in top views indicate hydrogen bonding involving side-chain amide groups.

side-chain amide carbonyl and main-chain amide NH groups in the same monomer units ($r_{H\cdots O} = 2.4 \pm 0.3$ Å, $\angle N-H\cdots O = 95 \pm 15°$, $\angle H\cdots O{=}C = 122 \pm 5°$), i.e., formation of four-center hydrogen bonds at the main-chain NH groups (Figure 9). It is also noted that consecutive three secondary $i/(i+3)$ hydrogen bonds in the main chain are broken, again leading to deformation of the α-helical main chain.

R6 is another periodic conformation composed of six monomer units with four hydrogen bonds formed in each period ($r_{H\cdots O} = 2.1 \pm 0.1$ Å, $\angle N-H\cdots O = 154 \pm 5°$, $\angle H\cdots O{=}C = 138 \pm 15°$), e.g., between the side-chain amide carbonyl group in the 19th (20th) monomer unit and the side-chain amide NH group in the 23rd (24th) monomer unit as well as between the side-chain amide NH group in the 21st (22nd) monomer unit and the main-chain amide carbonyl group in the 17th (18th) monomer unit, the latter giving four-center hydrogen bonding at the main-chain carbonyl group. At the same time, consecutive two $i/(i+3)$ main-chain hydrogen bonds in the main chain are broken as in **R3**.

The theoretical CD of **R3** in the ^1L_a band is found to be dominated by $i/(i+1)$ and $i/(i+4)$ exciton interactions of positive exciton chirality, i being any monomer

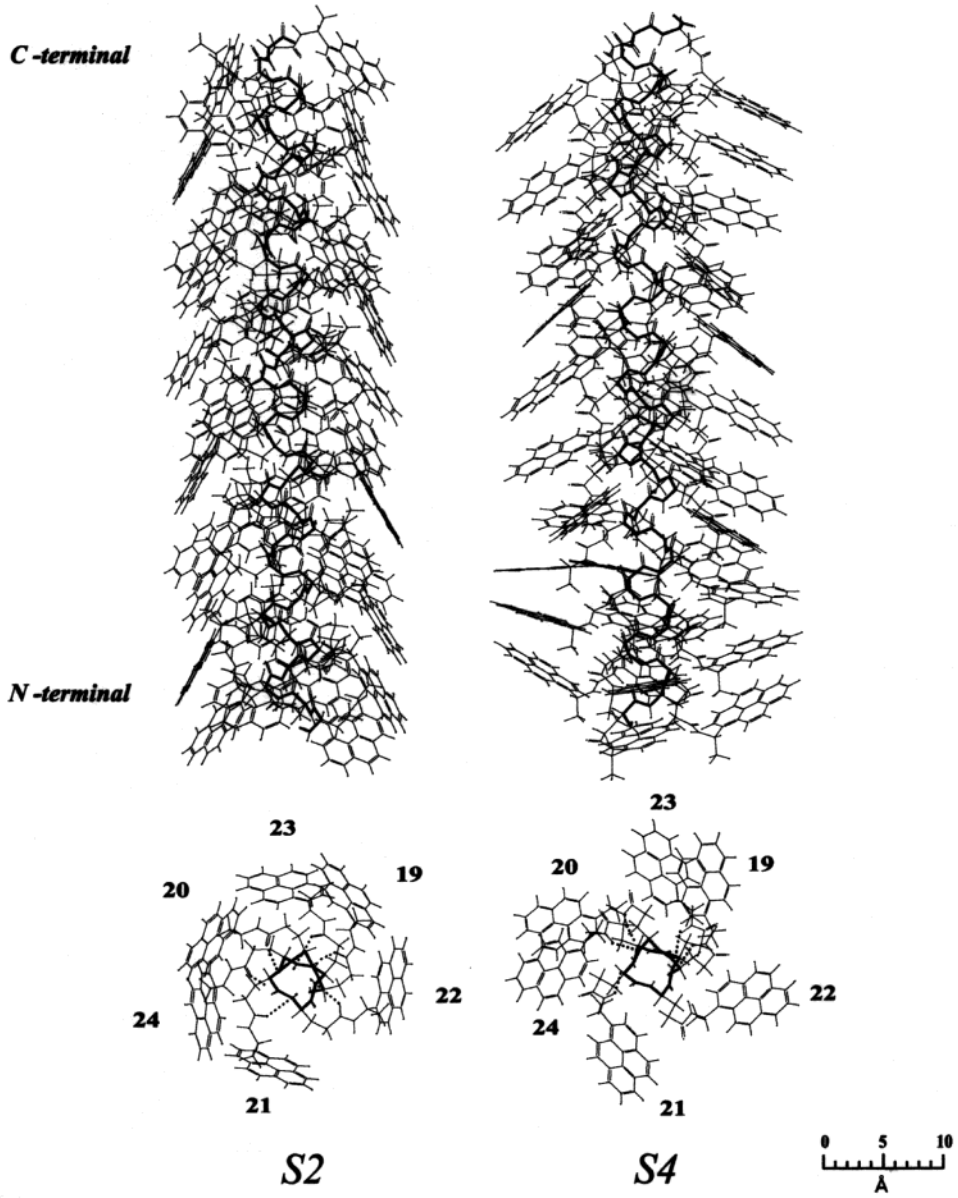

Figure 10. Side views and top views (six monomer units in the middle of polymer) of **S2** and **S4**. Dotted lines in top views indicate hydrogen bonding involving side-chain amide groups.

unit in the middle of the polymer (Figure 11). In the ^1B_b band, dominant $i/(i + 1)$ and $i/(i + 4)$ interactions give exciton coupling of positive and negative exciton chirality, respectively, which cancel one another and give little overall CD. **R3** thus gives calculated CD matching that observed with **1** in DMAc. (**1** in DMAc showed only the local chirality of side chain at the ^1B_b band, indicating no appreciable CD signals due to exciton coupling.) **R3** would thus be a candidate for the regulated conformation of **1** in DMAc.

The theoretical CD of **R5** in the ^1L_a band is found to be dominated by $i/(i + 3)$ and $i/(i + 4)$ exciton interactions of negative exciton chirality, matching CD observed with **1** in THF.[18] In the ^1B_b band, dominant $i/(i + 3)$ and $i/(i + 4)$ interactions give exciton coupling of negative exciton chirality and that of positive exciton chirality, respectively, giving very weak overall CD with exciton interaction of positive exciton chirality, which does not exactly match the CD observed in THF.

The theoretical CD of **R6** is similar to that of **R3** except that it has a weaker intensity in the ^1L_a band and weak CD with positive exciton coupling in the ^1B_b band.

Taking into account that the CD spectrum of **1** is sensitive to the hydrogen-bonding ability of the solvent, we presume that **R5**, which has side-chain amide NH groups available for hydrogen bonding by the solvent, changes to **R3** when the solvent is changed from THF to more strongly hydrogen-bonding DMAc.[18] Furthermore, as four of six side-chain amide N−H groups of **R6** are hydrogen-bonded to the main-chain or to the side-chain amide carbonyl groups, **R6** would not be affected so much by the solvent. Its contribution to CD in both solvents may not be excluded.

As for **2**, **S2** is a slightly periodic conformation with a period of six monomer units and has three consecutive continuous hydrogen bonds between the side-chain amide carbonyl group in the 18th (19th, 20th) monomer unit and the main-chain amide NH group in the 19th (20th, 21st) monomer unit ($r_{H\cdots O} = 2.4 \pm 0.2$ Å, $\angle N-H\cdots O = 93 \pm 10°$, $\angle H\cdots O{=}C = 121 \pm 3°$).

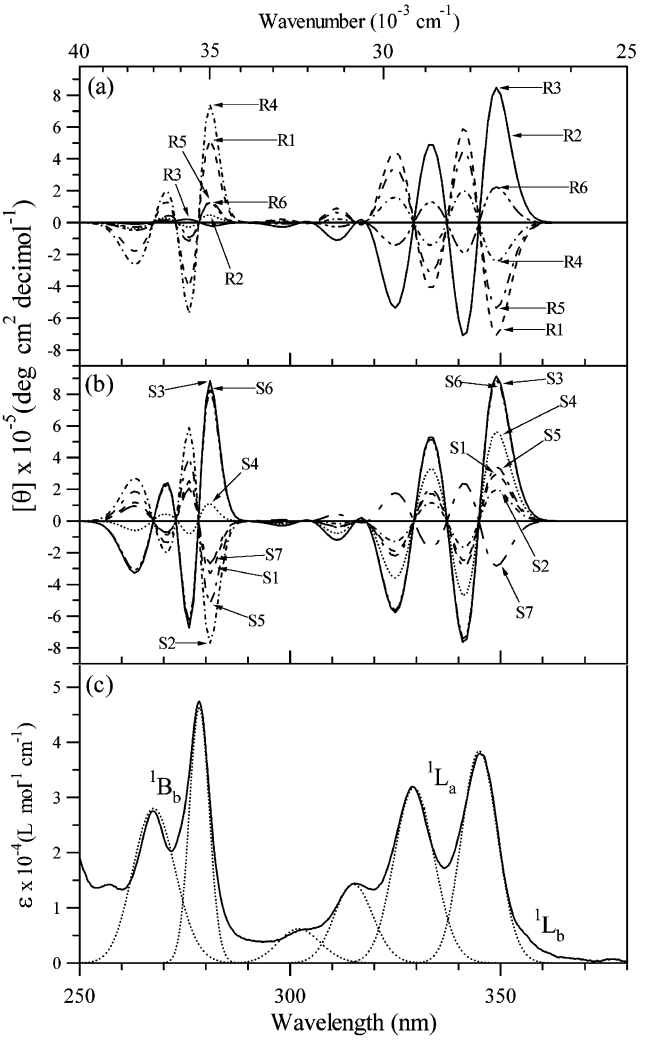

Figure 11. Theoretical CD spectra of (a) low-energy conformations of **1** and (b) those of **2**. UV absorption spectrum of **1** in DMAc (solid line) and that resolved into vibronic peaks using Gaussian functions (dotted line) are shown in part c.

S4 is a uniform conformation and has all the *i*th main-chain amide carbonyl groups hydrogen-bonded with the $(i + 4)$th side chain amide NH groups ($r_{H\cdots O} = 2.1 \pm 0.1$ Å, $\angle N-H\cdots O = 139 \pm 2°$, $\angle H\cdots O{=}C = 112 \pm 2°$). These hydrogen bonds are likely to be maintained in either solvent. At the same time, all the main-chain $i/(i + 3)$ hydrogen bonds are broken, and the main-chain amide carbonyl groups form new three-centered hydrogen bonds with the main-chain and side-chain amide NH groups.

The theoretical CD of **S2** gives dominant $i/(i + 4)$ exciton interactions of positive exciton chirality at the ^1L_a band and dominant $i/(i + 3)$ interactions of negative exciton chirality at the ^1B_b band, affording CD which does not match that observed with **2** in either solvent. The theoretical CD of **S4**, on the other hand, gives dominant $i/(i + 1)$ and $i/(i + 3)$ exciton interactions of positive exciton chirality at the ^1L_a band and dominant $i/(i + 1)$ and $i/(i + 4)$ interactions of positive exciton chirality at the ^1B_b band, which reproduce the CD of **2** observed in DMAc as well as in THF. We assume that **S4** is a strong candidate for the regulated structure of **2** in both solvents.

We believe that the highly controlled chromophore orientation is brought about by extensive hydrogen bonding between the side-chain amide NH and main-chain amide carbonyl groups as in **S4**. Such hydrogen bonds would have the side-chain pyrene chromophores located close to the main chain, giving densely populated and highly oriented chromophores along the helical main chain.

Conclusions

1 and **2** in DMAc, **2** in particular, gave strong CD signals in the pyrene absorption region as well as strong excimer emission. The temperature dependence of the CD spectra suggests that equilibrium is established between ordered and disordered side chains. The equilibrium constants estimated from the fluorescence decay indicate that **2** consistently has a smaller fraction of ordered side chains than **1** in the temperature range examined. The molar ellipticity of the ordered side chains of **2** was estimated to be 2.7 times as large as that of **1**. **2** thus apparently forms excimers more extensively due to the larger fraction of disordered side chains despite that the chromophore orientation is much better controlled in its ordered side chains. The possible ordered side-chain structures of **1** and **2**, evaluated by conformational analysis and theoretical CD calculations, suggest that the highly controlled chromophore orientation is brought about by extensive hydrogen bonding between the main-chain amide carbonyl and side-chain amide NH groups as in the regulated conformation of **2**, i.e., **S4**.

Acknowledgment. This work was supported by a Grant-in Aid for Scientific Research (Grant No. 10650863) from the Ministry of Education, Science, Sports, and Culture of Japan.

Supporting Information Available: Text giving the detailed synthesis of (*R* and *S*)-1-(1-pyrenyl)ethylamines and tables of X-ray crystallographic data and figures showing ORTEP diagrams of (*R*)-1-(1-pyrenyl)ethylammonium (1*S*)-(+)-10-camphorsulfonate. This material is available free of charge via the Internet at http://pubs.acs.org.

References and Notes

(1) Jordan, P.; Fromme, P.; Witt, H, T.; Klukas, O.; Saenger, W.; Krau, N. *Nature (London)* **2001**, *411*, 909.
(2) Zouni, A.; Witt, H.; Kern, J.; Fromme, P.; Krau, N.; Saenger, W.; Orth, P. *Nature (London)* **2001**, *409*, 739.
(3) McDermott, G.; Prince, S. M.; Freer, A. A.; Hawthornthwaite-Lawless, A. M.; Papiz, M. Z.; Cogdell, R. J.; Isaacs, N. W. *Nature (London)* **1995**, *374*, 517.
(4) Pispisa, B.; Stella, L.; Venanzi, M.; Palleschi, A.; Viappiani, C.; Polese, A.; Formaggio, F.; Toniolo, C. *Macromolecules* **2000**, *33*, 906.
(5) Pispisa, B.; Venanzi, M.; Palleschi, A.; Zanotti, G. *Macromolecules* **1994**, *27*, 7800.
(6) Inai, Y.; Sisido, M.; Imanishi, Y. *J. Phys. Chem.* **1991**, *95*, 3847.
(7) Sato, M.; Yoshimoto, M.; Nakahira, T.; Iwabuchi, S. *Makromol. Chem., Rapid Commun.* **1993**, *14*, 179.
(8) Egusa, S.; Sisido, M.; Imanishi, Y. *Macromolecules* **1985**, *18*, 882.
(9) Guillet, J. E. *Polymer Photochemistry and Photophysics: An introduction to the study of photoprocesses in macromolecules*; Cambridge University Press: Cambridge, England, 1985.
(10) Winnik, M. A. *Photophysical and photochemical tools in polymer science*; D. Reidel Publishing Co.: Amsterdam, 1985.
(11) Nakahira, T.; Ishizuka, S.; Iwabuchi, S.; Kojima, K. *Macromolecules* **1982**, *15*, 1217.
(12) Nakahira, T.; Ishizuka, S.; Iwabuchi, S.; Kojima, K. *Macromolecules* **1983**, *16*, 297.
(13) Irie, M.; Kamijo, T.; Aikawa, M.; Takemura, T.; Hayashi, K.; Baba, H. *J. Phys. Chem.* **1977**, *81*, 1571.

(14) Nakahira, T.; Fan, L.; Boon, C, T.; Fukada, T.; Karato, T.; Annaka, M.; Yoshikuni, M. *Polym. J.* **1998**, *30*, 910.
(15) Fan, L.; Fukada, T.; Annaka, M.; Yoshikuni, M.; Nakahira, T. *Polym. J.* **1999**, *31*, 364.
(16) Sato, M.; Morikawa, H.; Yoshimoto, M.; Nakahira, T.; Iwabuchi, S. *Nihon Kagaku Kaishi* **1992**, *11*, 1368.
(17) Shoji, O.; Okumura, M.; Kuwata, H.; Sumida, T.; Kato, R.; Annaka, M.; Yoshikuni, M.; Nakahira, T. *Macromolecules* **2001**, *34*, 4270.
(18) Shoji, O.; Nakajima, D.; Annaka, M.; Yoshikuni, M.; Nakahira, T. *Polymer* **2002**, *43*, 1711.
(19) Marcus, E.; Fitzpatrick, J. T. *J. Org. Chem.* **1960**, *25*, 199.
(20) Paul, N. *Optical Resolution Procedures for Chemical Compounds Vol. 1* Optical Resolution Information Center: New York, 1978.
(21) Toda, F.; Mori, K.; Okada, J.; Node, M.; Itoh, A.; Oomine, K.; Fuji, K. *Chem. Lett.* **1988**, 131.
(22) Altomare, A.; Burla, M. C.; Camalli, M.; Cascarano, G. L.; Giacovazzo, C.; Guagliardi, A.; Moliterni, A. G. G.; Polidori, G.; Spagna, R. *J. Appl. Crystallogr.* **1999**, *32*, 115.
(23) Beurskens, P. T.; Admiraal, G.; Beurskens, G.; Bosman, W. P.; de Gelder, R.; Israel, R.; Smits, J. M, M. *The DIRDIF-94 program system*; Technical Report of Crystallography Laboratory; University of Nijmegen: Nijmegen, The Netherlands, 1994.
(24) Sisido, M. *Pept. Chem.* **1991**, 105.
(25) Blundell, T.; Barlow, D.; Borkakoti, N.; Thornton, J. *Nature (London)* **1983**, *306*, 281.
(26) Liu, S. Y.; Purvis, G. D. *CAChe Molecular Mechanics Augmented Force Field*; Tektronix. Inc.: Beaverton, OR, 1991.
(27) Jeffrey, G. A. *An Introduction to Hydrogen Bonding*; Oxford University Press: Oxford, England,1997.
(28) Harada, N.; Nakanishi, K. *Circular Dichroic Spectroscopy: Exciton Coupling in Organic Stereochemistry*; University Science Books: New York and Tokyo-Kagaku Dojin, 1982.
(29) Ham, N. S.; Ruedenberg, K. *J. Chem. Phys.* **1956**, *25*, 13.
(30) Hochstrasser, R. M. *J. Chem. Phys.* **1960**, *33*, 459.
(31) Saeva, F. D.; Sharpe, P. E.; Olin, G. R. *J. Am. Chem. Soc.* **1973**, *95*, 7656.
(32) Birks, J. B. *Photophysics of Aromatic Molecules*; Wiley−Interscience, a division of John Wiley & Sons Ltd.: New York, 1970.
(33) Collart, P.; Toppet, S.; de Schryver, F. C. *Macromolecules* **1987**, *20*, 1266.

MA025922W